Robust control of the minima of high-order harmonics by fine-tuning the alignment of CO₂ molecules for shaping attosecond pulses and probing molecular alignment

Cheng Jin [1,*], Su-Ju Wang,[2] Song-Feng Zhao,[3] Anh-Thu Le,[4] and C. D. Lin[2]

[1]*Department of Applied Physics, Nanjing University of Science and Technology, Nanjing, Jiangsu 210094, China*

[2]*J. R. Macdonald Laboratory, Department of Physics, Kansas State University, Manhattan, Kansas 66506, USA*

[3]*Key Laboratory of Atomic and Molecular Physics and Functional Materials of Gansu Province, College of Physics and Electronic Engineering, Northwest Normal University, Lanzhou, Gansu 730070, China*

[4]*Department of Physics, Missouri University of Science and Technology, Rolla, Missouri 65409, USA*

In a recent paper [C. Jin, S.-J. Wang, X. Zhao, S.-F. Zhao, and C. D. Lin, Phys. Rev. A **101**, 013429 (2020)], we reported that the position and depth of the minima in the harmonic spectra of CO_2 molecules can be dramatically manipulated by a slight change of the degree of alignment, thus providing a convenient method of shaping attosecond pulses which could lead to the splitting of a typical single attosecond burst into two. Here, we demonstrate that harmonic minima can also be dramatically controlled by changing the pump-probe angles to shape attosecond pulses. In the meanwhile, since the pump-probe angle-dependent harmonic spectra are very sensitive to the degree of alignment, harmonic spectra can also be used to calibrate the alignment distribution of molecules. We identify such robust control of harmonic generation is due to the optical property of CO_2 and the coherent harmonic emission from the oriented molecules. The photoionization transition dipoles (PITDs) of CO_2 exhibit deep minima that change rapidly with molecular orientations accompanied by large phase changes of π in PITDs, thus leading to strong interference when the dipoles are added up coherently.

I. INTRODUCTION

High-order harmonic generation (HHG) resulting from the interaction of an intense laser field with molecular gases has opened up several research areas including high-harmonic spectroscopy (HHS) aiming at understanding molecular structure and electron correlations [1], as well as probing ultrafast dynamics in molecules [2–6]. Among the molecules, CO_2 is one of the favorites and has been studied in both experiments and theory extensively [7–29]. More recently, such studies in CO_2 have still mostly focused on the origin of minima in the harmonic spectra [30–33]. The best-known minimum in harmonic spectra is the one in Ar that occurs near a photon energy of about 50 eV [34–40]. The position of this minimum coincides well with the Cooper minimum in the photoionization spectra of Ar [41]. However, minima of HHG in molecules are quite ubiquitous and two types of minima have been widely addressed in the literature. One is called a "structural" minimum and the other is called a "dynamical" minimum. In the former the position of the minimum is mostly independent of the laser intensity or wavelength, while in the latter the position of the minimum would change with the laser intensity. Both types of minima can be understood in terms of harmonics generated from a single molecule and calculated accurately using the quantitative rescattering (QRS) theory [42–44], which is an extension of the well-known three-step model for the HHG.

According to the QRS theory, the laser-induced transition dipole for harmonic emission can be expressed as the product of a returning electron wave packet and the photorecombination (PR) transition dipole. The squared modulus of the amplitude of the returning electron wave packet is a smooth function of harmonic order and depends only on the property of the driving laser, while the photorecombination transition dipole (PRTD), which is related to the photoionization transition dipole (PITD), relies on the property of the target only. Since the first step of harmonic emission is tunnel ionization, at lower intensities, ionization and recombination would only occur for electrons in the highest occupied molecular orbital (HOMO). Thus, according to the QRS, minima in harmonic spectra would originate from the squared modulus of the PITD and the positions of such "structural" minima would not depend on the lasers used. As the laser intensity is increased, innershell electrons start to participate in the harmonic emission and their relative contributions increase quickly with increasing laser intensity. The induced harmonic emission dipoles from these multiple orbitals have to be added coherently and thus contribute to the so-called "dynamical" minima, whose positions vary with the laser intensity. Both "structural" and "dynamical" minima can be attributed to harmonics generated from a single molecule.

Experimentally, high harmonics observed in the laboratories are the consequence of coherent summation of induced transition dipoles weighted by the angular distribution of the molecules. In addition, the effect of propagation of harmonics in the gas medium has to be accounted for. The latter can be carried out by solving the Maxwell's wave equations. Both the

---

*Corresponding author: cjin@njust.edu.cn

coherent averaging of the induced dipoles over the alignment distribution and the macroscopic propagation in principle can modify the harmonic spectra [45–48], including the position of the minimum. Since very few theoretical calculations on HHG from molecules have been carried out, including these macroscopic effects, experimental HHG spectra are often interpreted based on the single-molecule model. However, calculations based on the QRS theory accompanied by treating all the macroscopic effects addressed above have been carried out for N_2 and CO_2 molecules and reported in earlier publications [40,49,50]. A prerequisite of the success of the QRS is the availability of accurate complex PITDs, $d(\omega,\theta)$. They are available for N_2 and CO_2 using state-of-the-art quantum chemistry codes.

In a recent paper [51], we examined the harmonic spectra of CO_2 from two earlier experiments of Vozzi *et al.* [22] and Rupenyan *et al.* [27]. In both experiments, the pump laser (for alignment) and the probe laser (for harmonic generation) were parallel and the degree of CO_2 alignment $\langle \cos^2 \theta \rangle$ was claimed to be 0.6, where θ is the angle between the molecular axis and the aligning laser polarization axis, yet the position of the harmonic minimum reported in Vozzi *et al.* [22] is at 60 eV while in Rupenyan *et al.* [27] it is located at 47 eV—a discrepancy of 13 eV. As reported in Ref. [51], the discrepancy was resolved by noting that the aligning laser and the temperature in the gas cell used in Vozzi *et al.* [22] are higher. According to our QRS simulation, for $\langle \cos^2 \theta \rangle = 0.55$, the minimum would occur at 47 eV, in agreement with Rupenyan *et al.* [27]. On the other hand, if we take $\langle \cos^2 \theta \rangle = 0.40$ at the gas cell, the minimum would occur at 60 eV, in agreement with Vozzi *et al.* [22]. At the same time, the simulation also gives a minimum deeper than that observed in Vozzi *et al.* [22]. The above results are surprising since if CO_2 molecules are isotropically distributed,

i.e., for $\langle \cos^2 \theta \rangle = 0.33$, the harmonic spectra do not have any minimum. To look for harmonic minima, experimentalists tend to use better-aligned molecules so nobody was tempted to measure harmonic spectra at $\langle \cos^2 \theta \rangle = 0.40$. As reported in Ref. [51], the deep minimum observed in Vozzi *et al.* [22] is the consequence of "enhancement" due to the coherent summation of transition dipoles from the angularly distributed molecules. The effect is very sensitive to the angular distributions of molecules. Such coherent enhancement is more efficient when molecules are not sharply distributed and depends critically on the nature of $d(\omega,\theta)$ of the target. It is especially significant in CO_2 since its dipole has a sharp minimum which is accompanied by a rapid phase change of π. Such a large phase change constitutes the constructive coherent sum of $d(\omega,\theta)$ over θ, thus resulting in a deep minimum within the harmonic spectra in a narrow photon energy range. The existence of such a deep and narrow minimum in the harmonic spectra is also accompanied by a large chirp in the phase of the harmonics, which in turn is reflected in the shaping of attosecond pulses, as addressed in Ref. [51].

In this work, we extend our previous work on the aligned CO_2 molecules. We investigate whether the shaping of attosecond pulses can be achieved if the pump-probe angle is varied, and we check if there are any interesting features in the perpendicular component of HHG with respect to the polarization of the probe laser. The paper is arranged as follows. In Sec. II, we briefly discuss the simulation methods and show the PITDs of the HOMO used in the simulations. In Sec. III, we first show some minima in the HHG spectra at different pump-probe angles, and we show the averaged PRTD versus the degree of alignment. We next demonstrate that attosecond pulses can be greatly shaped in two ways: either (i) by fixing the pump-probe angle and varying the alignment degree or (ii)
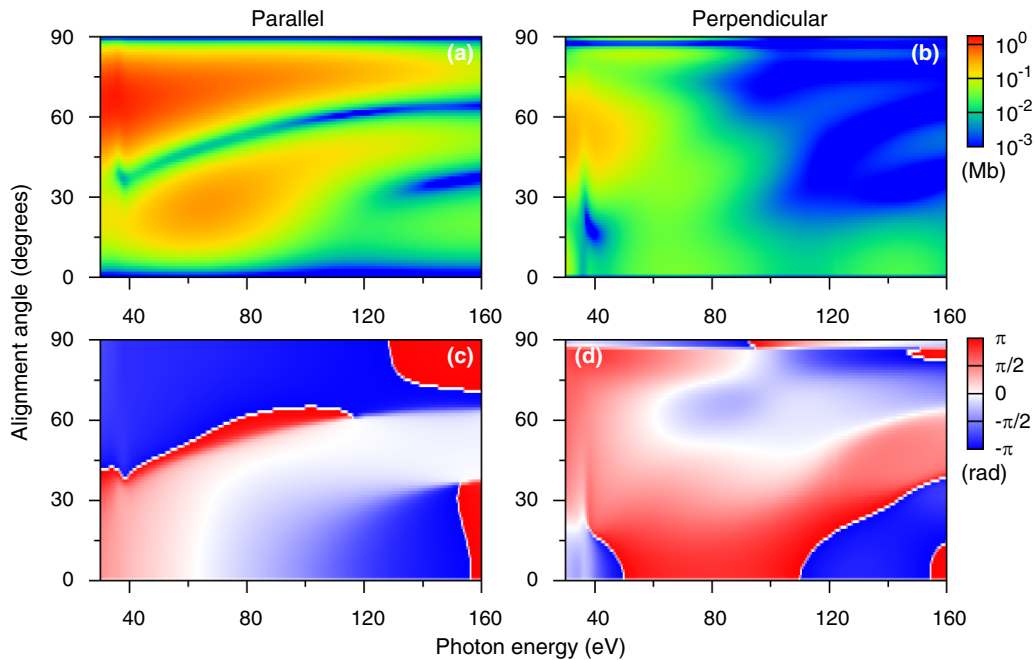
FIG. 1. Calculated differential photoionization cross sections [panels (a) and (b)] and phases [panels (c) and (d)] of the HOMO as a function of the alignment angle and the photon energy. Both the parallel and the perpendicular components of cross sections to the laser polarization direction are shown.

by fixing the alignment degree and changing the pump-probe angle. We then show how to use the harmonic minima to calibrate the molecular alignment. At the end, we examine the perpendicular component of high harmonics to the probe polarization direction. A short summary and outlook is given in Sec. IV.

II. DETAILS OF SIMULATION

To simulate HHG from aligned molecules that can be compared to experiments, there are three main steps. First, harmonics from each fixed-in-space molecule are calculated, including contributions from the HOMO as well as other inner orbitals if needed. This portion is carried out by using the QRS model. In this model, accurate photoionization transition dipoles are obtained from the state-of-the-art computer codes where the many-electron correlation effect is included. If multiple channels are contributing to the HHG, the harmonic amplitudes from these channels are added up coherently. Note that in the QRS model, the electrons are freed and recombined back to the same orbital. For CO_2, we consider electrons in the HOMO ($1\pi_g$), HOMO-1 ($1\pi_u$), and HOMO-2 ($3\sigma_u$) orbitals. Since molecules are not fixed in space, in the second step we average the single-molecule harmonic amplitudes weighted by the angular distribution, from which an averaged induced-dipole for a molecule is calculated. In the third step, since high harmonics are generated in the gas cell or the gas jet, one accounts for the propagation of the infrared laser and the emitted harmonics by solving the three-dimensional Maxwell's wave equations. The computational details of such calculations are given in Refs. [49,52]. In the present work, the fundamental driving laser field is not modified during its propagation in the gas medium. This is valid under the conditions of low gas pressure and low ionization level. Both the parallel and the perpendicular components of the high-harmonic field with respect to the polarization of the probe (or HHG generating) laser are calculated when the pump-probe angle is not zero.

For CO_2, prior calculations [27,49] have shown that high harmonics come mostly from the HOMO and HOMO-2 orbitals. In fact, for the laser intensity considered in this paper, the HOMO orbital is predominant. Some examples are given in Sec. III A.

In Fig. 1 we present the photoionization cross sections and their phases versus the photon energy and the alignment angle (between the molecular axis and the polarization axis of the aligning laser), for the initial HOMO state and for both the parallel and the perpendicular polarization components. These results are calculated with the MCCI package, developed by Lucchese [53,54] to study scattering and photoionization processes for linear molecules using the multi-channel Schwinger configuration interaction method. These results are expected to be superior to those from the EPOLYSCAT code [27,55,56], which is based on the Hartree-Fock method. The blue (dark) region in the upper graphs indicates that the cross sections are close to zero. For the parallel component, the cross sections go to zero at alignment angles of 0 and 90° because HOMO is a π_g orbital [see Fig. 1(a)]. In the middle region of Fig. 1(a), one can clearly see the presence of a minimum. The position (in energy) of the minimum moves to higher photon energy

as the alignment angle is increased. In the region of the minimum, one can observe a large dipole phase jump (from 0 to π or from $-\pi$ to 0) [see Fig. 1(c)]. However, one cannot find a minimum along the photon energy in Fig. 1(b) for the perpendicular direction except for the tiny one around 40 eV at small alignment angles. Figure 1 gives the essential structure information of CO_2 that is relevant for the HHG under investigation.

III. RESULTS AND DISCUSSIONS

A. Deep minima in the HHG spectra of aligned CO_2 molecules by varying pump-probe angle and alignment degree

In the previous study [51], we investigated the deep minimum at 60 eV for alignment with $\langle \cos^2 \theta \rangle = 0.40$ using wavelengths of 1.45, 1.6, and 1.7 μm under different laser intensities for parallel pump and probe pulses. Long-wavelength
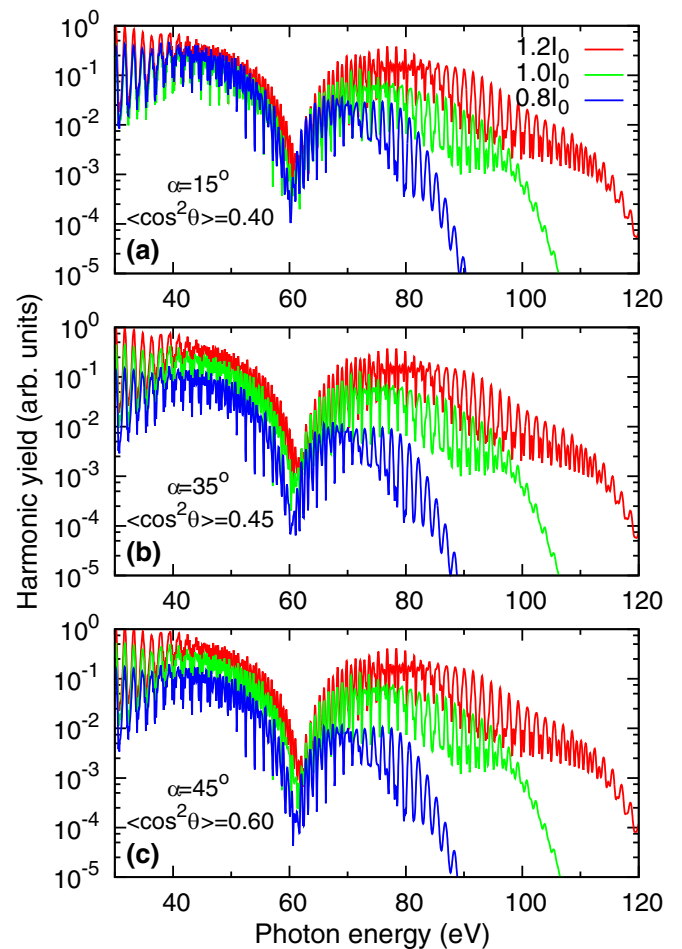
FIG. 2. Simulated macroscopic HHG spectra of aligned CO_2 molecules at different pump-probe angles α and alignment degrees $\langle \cos^2 \theta \rangle$ (as indicated in the figures). Laser intensity at the center of the gas jet (indicated with $I_0 = 10^{14}$ W/cm^2) for three spectra are indicated. Both the HOMO and the two inner orbitals are included in the simulations. Only the parallel component to the polarization direction of the probe laser is shown. See text for additional laser parameters. In each figure, from top to bottom, the spectra are for laser intensities of 1.2, 1.0, and 0.8 I_0, respectively.
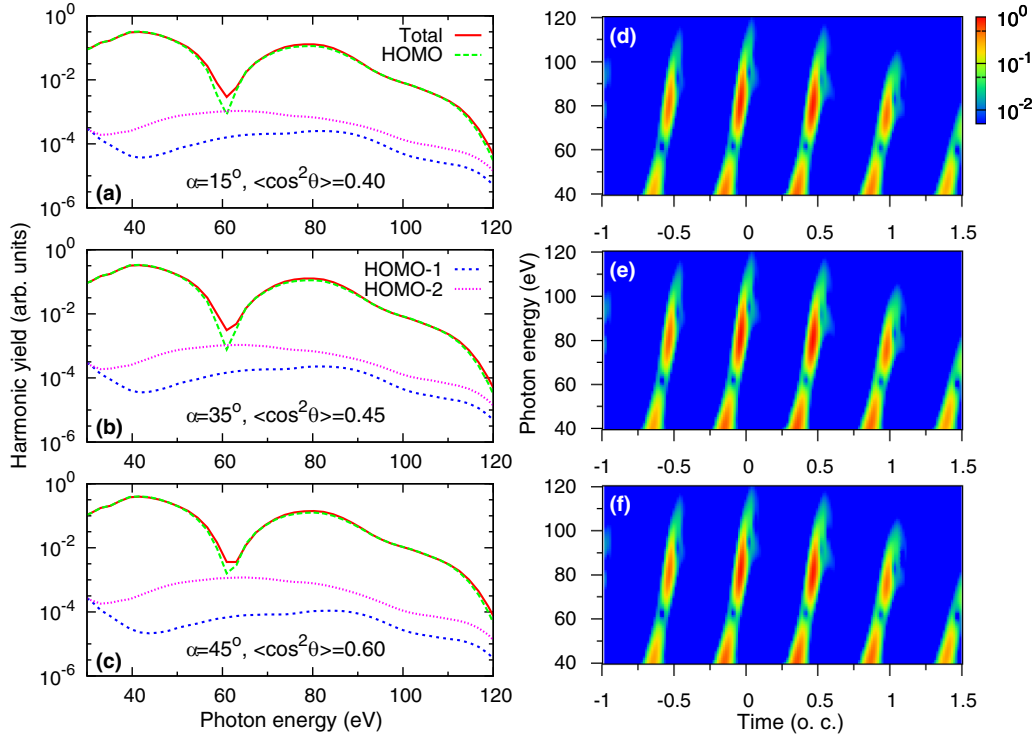
FIG. 3. (a)–(c) Comparison of the relative contributions of harmonics from different molecular orbitals. The spectra are smoothed by using Bezier curves. The gas jet is located after laser focus. (d)–(f) Time-frequency analysis of macroscopic harmonic emissions at the off-axis position ($r = w_0/3$) of the exit plane for harmonics in panels (a)–(c), respectively. w_0 is the beam waist of the generating laser and o.c. stands for the optical cycle of the 1600-nm laser.

lasers were used to obtain a larger spectral range. The HHG comes primarily from the HOMO. In this work, our main purpose is to examine HHG and attosecond pulses when the pump and probe pulses are not parallel. We fix the laser wavelengths at 1.6 μm, the carrier-envelope phase (CEP) at 0, and pulse durations of four optical cycles. The laser beam waist (at the focus) is assumed to be $w_0 = 35\ \mu$m, and the gas jet is located 3 mm after the laser focus. Its length is set at 0.5 mm, and its distribution in the laser-gas interaction region is uniform. The harmonic yields are integrated over the radial direction at the exit plane of the gas medium. The polarization direction of the HHG generating probe laser is varied with respect to the aligning one. The degree of alignment by a weak 800-nm pump (or aligning) laser is also adjusted. The time delay between the pump and probe lasers is fixed at the first half-revival when CO_2 molecules are best aligned.

The simulated macroscopic HHG spectra are shown in Fig. 2 for different pump-probe angles α. Figure 2(a) shows that a harmonic minimum at 60 eV can be obtained for $\alpha = 15°$ with $\langle \cos^2 \theta \rangle = 0.40$. Its position does not change when the laser intensity is changed. The same minimum at 60 eV can be reached by $\alpha = 35°$ with $\langle \cos^2 \theta \rangle = 0.45$, as seen in Fig. 2(b), and by $\alpha = 45°$ with $\langle \cos^2 \theta \rangle = 0.60$, as seen in Fig. 2(c). Again, using other laser intensities does not change the position of the minimum.

In Figs. 3(a)–3(c), we demonstrate that the minimum is slightly "filled" if the contributions from HOMO-1 and HOMO-2 are added. Figures 3(d)–3(f) show that the harmonics calculated predominantly come from short-trajectory electrons, as seen in the time-frequency analysis in the

figures. Since the gas jet is located after the laser focus, good phase-matching is achieved and long-trajectory electron emissions are effectively removed. This configuration has been commonly implemented in experiments for the generation of attosecond pulses to ensure well-behaved temporal pulses are obtained. These test calculations validate the following analysis with the harmonics from the HOMO only for one common laser intensity.

B. Tracking the harmonic minimum via the averaged PR transition dipole

Similar to the QRS theory, macroscopic harmonic yields can be expressed as [52,57]

$$S_{\mathrm{h}}^{\parallel,\perp}(\omega, \alpha) \propto \omega^4 |W'(\omega)|^2 |d_{\mathrm{avg}}^{\parallel,\perp}(\omega, \alpha)|^2, \qquad (1)$$

where $W'(\omega)$ is a "macroscopic wave packet," and $d_{\mathrm{avg}}^{\parallel,\perp}(\omega, \alpha)$ is the averaged PR transition dipole, which is defined as

$$d_{\mathrm{avg}}^{\parallel,\perp}(\omega, \alpha) = \int_0^\pi N(\theta')^{1/2} d^{\parallel,\perp}(\omega, \theta') \rho(\theta', \alpha) \sin \theta'\, d\theta'. \quad (2)$$

Here, $N(\theta')$ is the ionization probability [58,59], $\rho(\theta', \alpha)$ is the angular distribution (in the probe-laser frame) for the pump-probe angle α, and $d^{\parallel,\perp}(\omega, \theta')$ is the parallel or perpendicular (to the probe-laser polarization) component of the PR transition dipole. θ' is the angle between the molecular axis and the polarization direction of the probe laser, and $\rho(\theta', \alpha)$ can be calculated through a transformation from the pump frame to the probe one [60], using an angular distribution $\rho(\theta)$ by the aligning laser. Note that the averaged PR
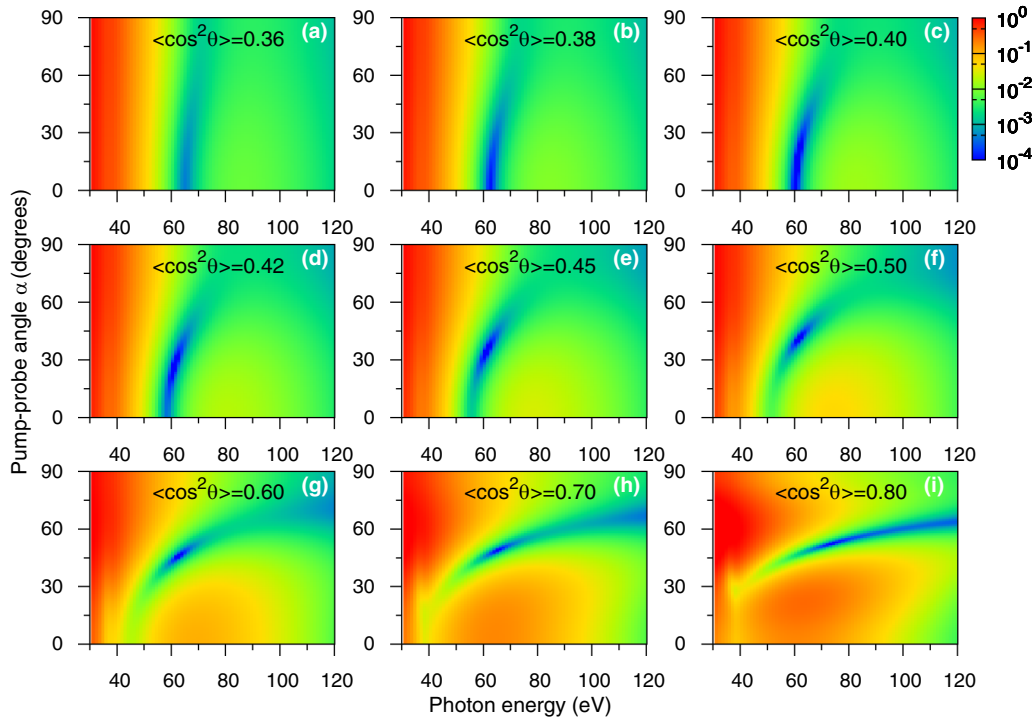
FIG. 4. Averaged photorecombination transition dipoles (the squared modulus) of the HOMO vs the pump-probe angle and the photon energy for different alignment degrees $\langle \cos^2 \theta \rangle$. Only the parallel polarization component is shown.

transition dipole for each molecule is calculated coherently. Since $W'(\omega)$ varies smoothly with the photon energy, any features in the macroscopic HHG can be related to those in the averaged PR transition dipole.

We show in Fig. 4 the dependence of $|d_{avg}^{\parallel}(\omega, \alpha)|^2$ on the pump-probe angle for selected alignment distributions, where the alignment degrees $\langle \cos^2 \theta \rangle$ are given from 0.36 (close to 0.33 for the isotropic distribution) to 0.8 (close to 1.0 for the perfect alignment). Blue (dark) regions indicate that the squared modulus of the averaged PRTDs (or harmonic yields) are very small, which are caused by a coherent average over alignment angles. One can see that the region of the minimum changes rapidly as $\langle \cos^2 \theta \rangle$ is increased. From Figs. 4(c), 4(e), and 4(g), we can identify the minima around 60 eV at the pump-probe angles of 15°, 35°, and 45°, respectively, which are responsible for the minima in the harmonic spectra in Fig. 2. Furthermore, there is a minimum constantly located around 60 eV by varying the pump-probe angle if the alignment degree is not larger than 0.7. Comparing to Fig. 1(a), the averaged PRTDs are quite different from the dipole for fixed-in-space molecules. Only for the highly aligned case of $\langle \cos^2 \theta \rangle = 0.80$ can we see the averaged dipole is close to the fixed-in-space ones.

C. Shaping of attosecond pulses in two ways

As discussed in Ref. [51], a deep minimum in the HHG spectra would split one regular attosecond burst into two in the time domain. To locate the deep minimum, one can manipulate the pump-probe angle and the degree of alignment. Accordingly, we show the lineouts of $|d_{avg}^{\parallel}(\omega, \alpha)|^2$ in Fig. 4 in two different ways.

First, in Figs. 5(a)–5(c), we show $|d_{avg}^{\parallel}(\omega, \alpha)|^2$ for different alignment degrees at fixed pump-probe angles of 15°, 35°, and 45°, respectively. At $\alpha = 15°$, the harmonic minimum shifts from 63 to 52 eV as $\langle \cos^2 \theta \rangle$ changes from 0.38 to 0.50. Similar large shifts of the position of minimum with $\langle \cos^2 \theta \rangle$ over the same range can be seen for $\alpha = 35°$ and $\alpha = 45°$, respectively. Figures 5(d)–5(f) show the corresponding phases of $d_{avg}^{\parallel}(\omega, \alpha)$. It is noted that each harmonic minimum is accompanied by a rapid phase change close to π. The deeper the minimum is, the narrower the energy region is where such a phase change of π occurs.

In Fig. 6, attosecond pulses synthesized from high harmonics containing the minimum are shown over one half optical cycle of the 1600-nm laser. If the energy range of high harmonics is truncated to between 56 and 66 eV as in Figs. 6(a)–6(c), the attosecond pulse in the time domain begins to split from a single burst into two, with the two bursts of nearly equal strength occurring when the harmonic minimum is deepest. The change occurs within a small variation of alignment. Alternatively, if the harmonics with a bandwidth of 10 eV centered at the minimum are synthesized for each $\langle \cos^2 \theta \rangle$, every attosecond pulse is split into two bursts, as demonstrated in Figs. 6(d)–6(f).

A second way to efficiently control the generation of attosecond pulses is to tune the pump-probe angles at a fixed alignment. In Figs. 7(a)–7(c), we show how $|d_{avg}^{\parallel}(\omega, \alpha)|^2$ vary with the pump-probe angle for three alignments with $\langle \cos^2 \theta \rangle$ fixed at 0.40, 0.50, and 0.60. The harmonic spectra clearly reveal extreme variations with the change of the pump-probe angle. Such changes in the harmonic spectra are accompanied by large changes of the harmonic phases across the minimum as demonstrated in Figs. 7(d)–7(f) and the generation of
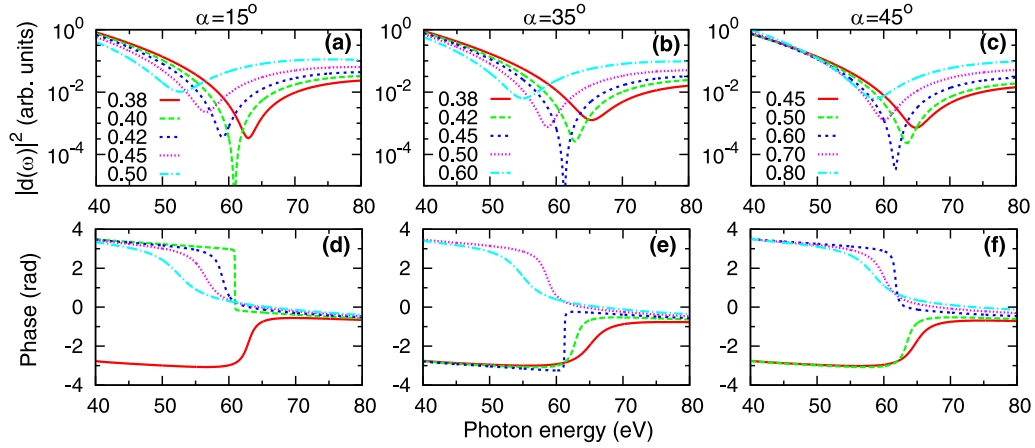
FIG. 5. (a)–(c) Averaged PR transition dipoles (the squared modulus) and (d)–(f) their phases, for the HOMO and the parallel component only, vs the photon energy, for different degrees of alignment (as shown in the labels). Pump-probe angles α are given on the top of the panels.

attosecond pulses with two split bursts in the time domain as shown in Figs. 7(g)–7(i).

In short, these results demonstrate how harmonic spectra in CO_2 molecules can be dramatically controlled with small changes in the degree of alignment. Together with the earlier results reported in Ref. [51], such control of harmonic spectra is readily observed by either varying the degree of alignment in fine steps at a fixed pump-probe angle or fine-tuning the pump-probe angles at a given alignment degree. Such robust control is possible because the PITD of CO_2, $d(\omega, \theta)$, for the HOMO orbital [see Fig. 1(a)] has a strong minimum whose position changes rapidly with θ. Since such a minimum is always accompanied by a large variation of phase by π, and the fact that harmonics generated in the gas cell add $d(\omega, \theta)$ coherently weighted by the alignment distributions of molecules, this results in a $|d_{avg}^{\|}(\omega, \alpha)|^2$ that changes rapidly with the degree of alignment and the pump-probe angle. Such strong sensitivity in the harmonic spectra has not been carefully examined experimentally, nor have the predicted shaped attosecond pulses been characterized or used in applications.

D. Calibrating the degree of molecular alignment

The strong dependence of HHG spectra on the angular distributions of CO_2 molecules may be utilized as a sensitive probe of molecular alignment. In Figs. 8(a)–8(c), we show the HHG spectra calculated at three pump-probe angles of $15°$, $30°$, and $40°$. For each order, the harmonics are slightly shifted from each other for easier visualization. The results are shown for three alignment distributions with $\langle \cos^2 \theta \rangle = 0.40$, 0.45, and 0.50, respectively. For each fixed alignment distribution with respect to the pump laser, the harmonic minimum and the spectra change significantly as the pump-probe angle is varied. From Eq. (2), their changes are due to the weighted coherent average of the angular distributions of molecules $\rho(\theta', \alpha)$ varying with the pump-probe angle α. With respect to the aligning laser polarization axis, the alignment distribution is represented by $\rho(\theta)$. By taking spectra like Fig. 8(a), for example, the harmonic spectra measured are proportional to the modulus square of Eq. (2). Thus the two-dimensional harmonic spectra, in pump-probe angle and harmonic order, can be used to retrieve the one-dimensional function $\rho(\theta)$
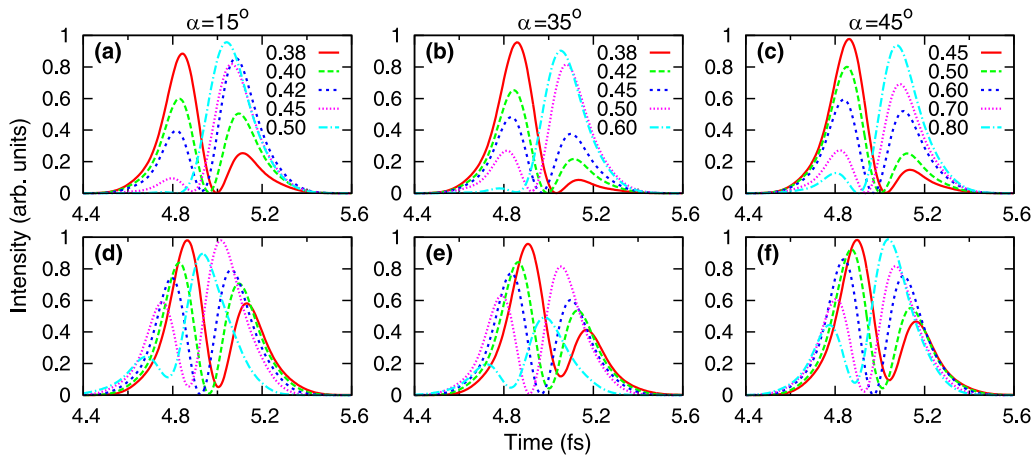
FIG. 6. Attosecond pulses synthesized by off-axis ($r = w_0/3$) harmonics from 56 to 66 eV [panels (a)–(c)] or by harmonics centered at the minimum with a bandwidth of 10 eV [panels (d)–(f)]. A Gaussian envelope is applied to harmonics beyond the boundary for smooth cutoff. In each figure, some factors may have been multiplied for easy comparison. Macroscopic propagation is included with laser parameters the same as those in Fig. 2 for 1600 nm and $1.2\, I_0$. Pump-probe angles are given on the top of the panels.
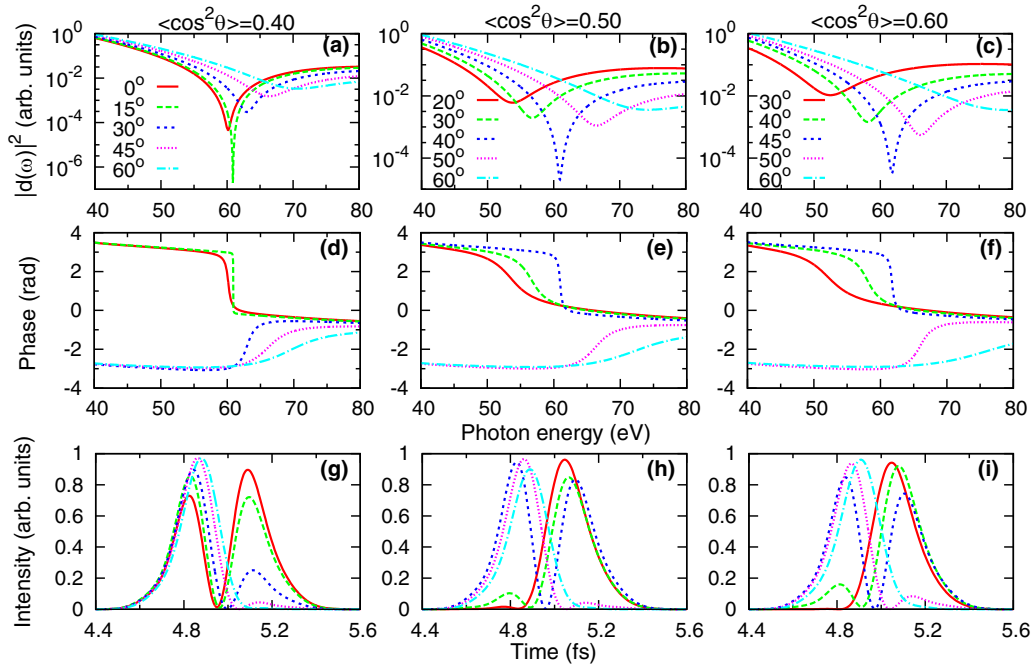
FIG. 7. Same as Fig. 5 and Figs. 6(a)–6(c) except that the pump-probe angles are varied (as shown by labels). Degrees of alignments $\langle \cos^2 \theta \rangle$ are given on the top of the panels. The attosecond pulses are synthesized from high harmonics covering from 56 to 66 eV [panels (g) and (h)] and from 57 to 67 eV [panel (i)].

readily if one assumes that the ionization rate and PRTDs for fixed-in-space molecules are known from theory. For the well-studied CO_2 molecules, it is reasonable to make such

assumptions. To test whether the retrieved $\rho(\theta)$ is correct, one can use a probe laser of different intensity or wavelength to generate harmonics and check if the observed harmonic
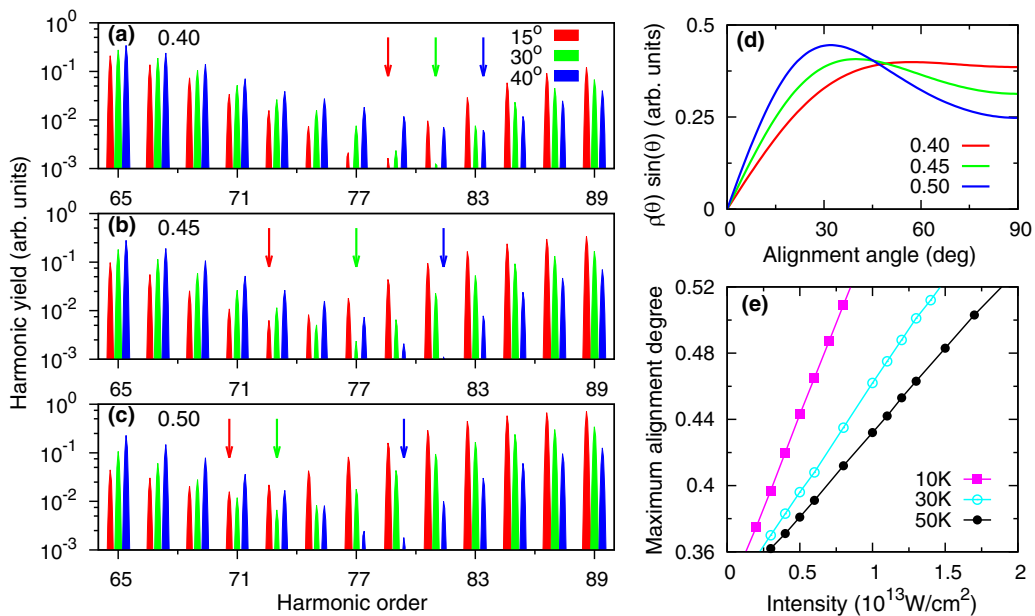
FIG. 8. Macroscopic HHG spectra obtained with the same fixed laser conditions as those in Fig. 2 at three pump-probe angles of $15°$, $30°$, and $45°$, for three alignments of $\langle \cos^2 \theta \rangle = 0.40$, 0.45, and 0.50, respectively. Only the parallel polarization components are shown. The arrows indicate the positions of minima in the spectra. The simulated spectra are smoothed by a Gaussian function centered at the odd harmonics. The harmonics with the same order but different pump-probe angles are shifted for easy comparison; at each order the harmonic peaks are for $15°$, $30°$, and $45°$ (from left to right), respectively. (d) Weighted angular distributions of molecules for the three alignments. Between $60°$ and $90°$, from top to bottom, the distributions are for alignment degrees of 0.40, 0.45, and 0.50, respectively. (e) Maximal alignment expressed in terms of $\langle \cos^2 \theta \rangle$ at the first half-revival as a function of laser intensity when the gas temperature is fixed (as shown in the figure). The aligning laser has a wavelength of 800 nm and a duration of 100 fs.
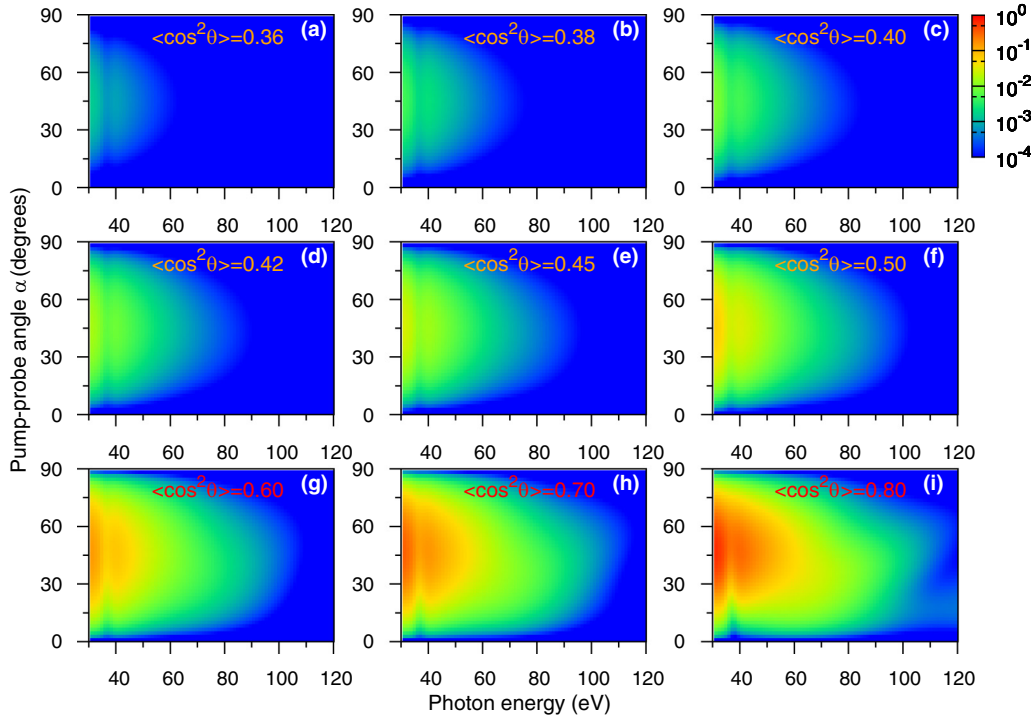
FIG. 9. Same as Fig. 4 but for the polarization component perpendicular to the probe-laser polarization.

spectra can be reproduced from calculations using the previously retrieved molecular alignment distribution $\rho(\theta)$.

Next one can change the intensity of the pump laser to obtain a different alignment distribution. By taking the harmonic spectra for different pump-probe angles, one can again retrieve the new $\rho(\theta)$. Experimentally, it is relatively easy to measure the change of laser power of the aligning laser, or the relative peak intensity if the focusing condition stays the same. From the two retrieved alignment distributions, one would be able to retrieve the temperature of the gas in the cell. Figure 8(e) shows how $\langle\cos^2\theta\rangle$ changes with the pump-laser intensity for three different gas temperatures. This figure is obtained by assuming that the alignment distribution of molecules can be calculated using the rigid-rotor model [61,62]. It shows that $\langle\cos^2\theta\rangle$ varies essentially linearly with the temperature in the gas cell. Using the ratio of $\langle\cos^2\theta\rangle$ for the two retrieved alignment distributions and Fig. 8(e), one can easily obtain the temperature of the gas cell. In addition, if the intensity of the pump laser is further increased, the molecules may be vibrationally excited. When this happens, the rigid-rotor model would fail to describe the alignment distributions and the linear dependence seen in Fig. 8(e) would be changed. Experimentally it will be of great interest to see how it changes. Of course the harmonic spectra would also undergo significant change. The strong dependence of harmonic spectra on the alignment distribution can be used to probe the rovibrational excitations of CO_2 which have not been carefully examined so far experimentally. We emphasize that the harmonic spectra reported here are not sensitive to the probe-laser intensity so long it does not excite harmonics from innershell orbitals. Clearly, the discussion presented in this section is still sketchy. It is presented here to stimulate further future theoretical and experimental investigations.

E. Perpendicularly polarized high-order harmonics

For aligned molecules, it is well known that high harmonics have perpendicular components if the pump-probe angle is not equal to zero [63–66]. The minima of harmonics addressed so far are only for the parallel component (with respect to the polarization of the probe laser); it is natural to ask whether the minima will be filled by the perpendicular component. This can be checked by calculating the averaged PR transition dipoles in the perpendicular direction. In Fig. 9, we show $|d_{avg}^{\perp}(\omega, \alpha)|^2$ as a function of both the photon energy and the pump-probe angle at nine fixed alignment distributions. Note that the plots are drawn using the same scale as the parallel components shown in Fig. 4 for easy direct comparisons. Clearly, there is no evidence of minima in $|d_{avg}^{\perp}(\omega, \alpha)|^2$, and thus there are no minima in the perpendicular harmonics in the angular and photon energy region considered. One can also see that the PRTD is more symmetric about $45°$ for weak alignment than for strong alignment. The difference appears because the angular distribution $\rho(\theta', \alpha)$ in Eq. (2) changes when the pump-probe angle α is varied.

The existence of nonzero perpendicular harmonic components can fill up the minimum in the parallel component if the experiment does not distinguish the two polarizations, unless the perpendicular component is small. This occurs for small pump-probe angles. We have carried out HHG spectrum simulations including the propagation effect for both polarizations, for several combinations of alignments and pump-probe angles, as shown in Fig. 10. Only for small pump-probe angles can one neglect the perpendicular polarization components. For harmonics generated at larger pump-probe angles, to observe the results reported here, polarizers will be needed to single out the parallel polarization harmonics. In
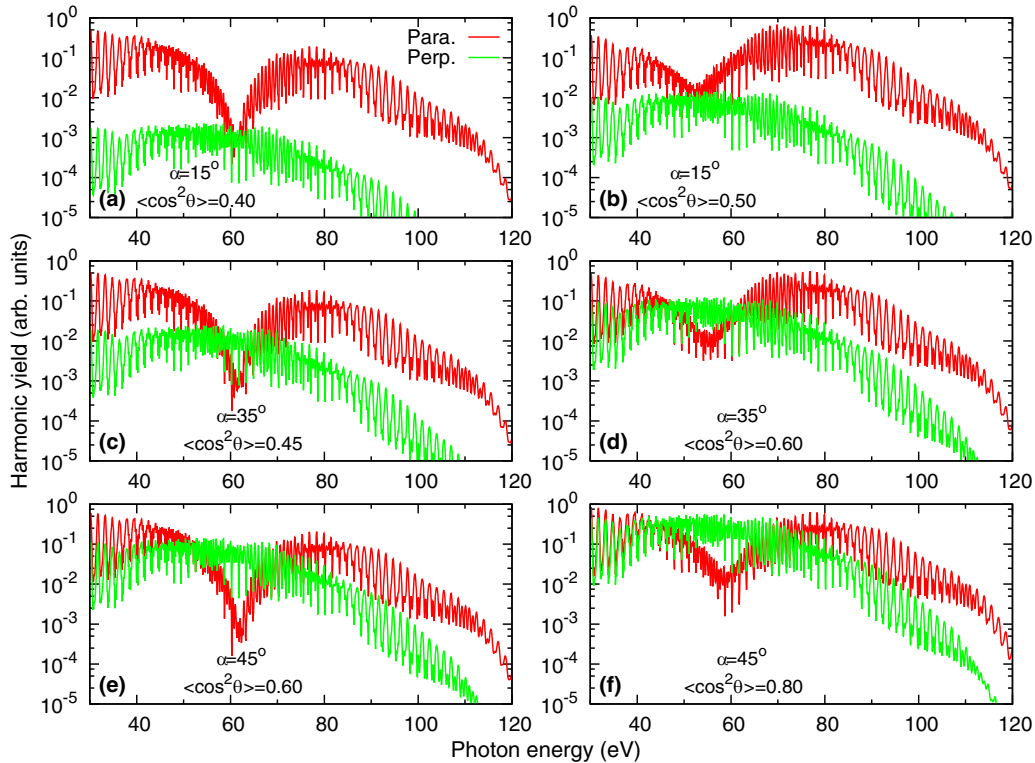
FIG. 10. Comparison of the parallel and perpendicular components (upper and lower ones except for the 60-eV region) of HHG spectra to the polarization direction of the generating laser. The results are shown for different combinations of pump-probe angle and alignment degree (as indicated in the figures). In the simulations, both the HOMO and the two inner orbitals are included. The macroscopic conditions are the same as those in Fig. 2 for 1600 nm and 1.2 I_0.

experiments where polarization is not selected, the minima of high harmonics addressed in this article would not be visible unless the harmonics are collected for the parallel pump and probe geometry only.

IV. SUMMARY AND OUTLOOK

In this work, we have investigated deep minima in the high-order harmonic generation of aligned CO_2 molecules by varying the pump-probe angle and the alignment distributions. These minima are caused by the minima in the photoionization transition dipole $d(\omega, \theta)$ of a fixed-in-space molecule. While $d(\omega, \theta)$ is the most fundamental complex-valued quantity in the photoionization process, it has never been directly probed in synchrotron radiation experiments. In particular, the complex structure of $d(\omega, \theta)$ predicted by state-of-the-art quantum chemistry calculations has never been verified in experiments, for example, the existence of a sharp minimum in $d(\omega, \theta)$, together with its phase. Such information, as illustrated in this work, can be revealed by measuring the harmonic spectra from aligned CO_2 molecules. By taking advantage of the coherent emissions of harmonics, a great wealth of harmonic spectra can be obtained by changing the pump-probe angle and the degree of alignment. Not only $d(\omega, \theta)$ in the molecular frame can be extracted in the future; we also pointed out that the wealth of harmonic spectra can be used to interrogate the details of rotational wave packets generated by the aligning pulse

and that shaped attosecond pulses can be synthesized using a broadband of harmonics near the minimum of the harmonic spectra. While high harmonics generated from CO_2 molecules have been investigated for nearly two decades, the rich physics that has been extracted from harmonic spectra is still just the tip of an iceberg. Clearly, further dedicated experiments would help unravel the "hidden" information in the HHG spectra.

In the future, shaped attosecond pulses could play an important role for their applications in science and technology [67]. Although CO_2 has been identified as a working medium, other molecules like N_2, O_2, or N_2O probably can be used to shape attosecond pulses as well, since they all show the minima in the HHG spectra [21,27,68]. With the development of midinfrared laser technology [69–71], efficient HHG and isolated attosecond pulses have been demonstrated in soft x rays [72–76]. It will be interesting to demonstrate whether the shaping of soft x-ray attosecond pulses can be realized by using aligned or oriented molecules. Finally, it will be of interest to investigate the polarization property of shaped attosecond pulses in the nonparallel pump-probe geometry [77].

---

[1] P. M. Kraus and H. J. Wörner, Angew. Chem., Int. Ed. **57**, 5228 (2018).

[2] F. Krausz and M. Ivanov, Rev. Mod. Phys. **81**, 163 (2009).

[3] F. Calegari, G. Sansone, S. Stagira, C. Vozzi, and M. Nisoli, J. Phys. B **49**, 062001 (2016).

[4] L.-Y. Peng, W.-C. Jiang, J.-W. Geng, W.-H. Xiong, and Q. Gong, Phys. Rep. **575**, 1 (2015).

[5] J. P. Marangos, J. Phys. B **49**, 132001 (2016).

[6] H. Yun, S. J. Yun, G. H. Lee, and C. H. Nam, J. Phys. B **50**, 022001 (2017).

[7] M. Lein, N. Hay, R. Velotta, J. P. Marangos, and P. L. Knight, Phys. Rev. Lett. **88**, 183903 (2002).

[8] R. de Nalda, E. Heesel, M. Lein, N. Hay, R. Velotta, E. Springate, M. Castillejo, and J. P. Marangos, Phys. Rev. A **69**, 031804(R) (2004).

[9] T. Kanai, S. Minemoto, and H. Sakai, Nature (London) **435**, 470 (2005).

[10] C. Vozzi et al., Phys. Rev. Lett. **95**, 153902 (2005).

[11] A. T. Le, X. M. Tong, and C. D. Lin, Phys. Rev. A **73**, 041402(R) (2006).

[12] M. Gühr, B. K. McFarland, J. P. Farrell, and P. H. Bucksbaum, J. Phys. B **40**, 3745 (2007).

[13] N. Wagner, X. Zhou, R. Lock, W. Li, A. Wüest, M. Murnane, and H. Kapteyn, Phys. Rev. A **76**, 061403(R) (2007).

[14] Y. J. Chen and J. Liu, Phys. Rev. A **77**, 013410 (2008).

[15] W. Boutu et al., Nat. Phys. **4**, 545 (2008).

[16] T. Kanai, E. J. Takahashi, Y. Nabekawa, and K. Midorikawa, Phys. Rev. A **77**, 041402(R) (2008).

[17] X. Zhou, R. Lock, W. Li, N. Wagner, M. M. Murnane, and H. C. Kapteyn, Phys. Rev. Lett. **100**, 073902 (2008).

[18] O. Smirnova, Y. Mairesse, S. Patchkovskii, N. Dudovich, D. Villeneuve, P. Corkum, and M. Yu. Ivanov, Nature (London) **460**, 972 (2009).

[19] P. Wei, P. Liu, J. Chen, Z. Zeng, X. Guo, X. Ge, R. Li, and Z. Xu, Phys. Rev. A **79**, 053814 (2009).

[20] R. Torres et al., Phys. Rev. A **81**, 051802(R) (2010).

[21] H. J. Wörner, J. B. Bertrand, P. Hockett, P. B. Corkum, and D. M. Villeneuve, Phys. Rev. Lett. **104**, 233904 (2010).

[22] C. Vozzi, M. Negro, F. Calegari, G. Sansone, M. Nisoli, S. De Silvestri, and S. Stagira, Nat. Phys. **7**, 822 (2011).

[23] K. Kato, S. Minemoto, and H. Sakai, Phys. Rev. A **84**, 021403(R) (2011).

[24] J. Li, P. Liu, H. Yang, L. Song, S. Zhao, H. Lu, R. Li, and Z. Xu, Opt. Express **21**, 7599 (2013).

[25] X. Zhu, M. Qin, Y. Li, Q. Zhang, Z. Xu, and P. Lu, Phys. Rev. A **87**, 045402 (2013).

[26] A. Rupenyan, P. M. Kraus, J. Schneider, and H. J. Wörner, Phys. Rev. A **87**, 031401(R) (2013).

[27] A. Rupenyan, P. M. Kraus, J. Schneider, and H. J. Wörner, Phys. Rev. A **87**, 033409 (2013).

[28] M. Qin, X. Zhu, Y. Li, Q. Zhang, P. Lan, and P. Lu, Opt. Express **22**, 6362 (2014).

[29] J. Guo, X.-L. Ge, H. Zhong, X. Zhao, M. Zhang, Y. Jiang, and X.-S. Liu, Phys. Rev. A **90**, 053410 (2014).

[30] H. Yun, K.-M. Lee, J. H. Sung, K. T. Kim, H. T. Kim, and C. H. Nam, Phys. Rev. Lett. **114**, 153901 (2015).

[31] B. D. Bruner et al., Faraday Discuss. **194**, 369 (2016).

[32] N. Suárez, A. Chacón, J. A. Pérez-Hernández, J. Biegert, M. Lewenstein, and M. F. Ciappina, Phys. Rev. A **95**, 033415 (2017).

[33] M. Ruberti, P. Decleva, and V. Averbukh, Phys. Chem. Chem. Phys. **20**, 8311 (2018).

[34] H. J. Wörner, H. Niikura, J. B. Bertrand, P. B. Corkum, and D. M. Villeneuve, Phys. Rev. Lett. **102**, 103901 (2009).

[35] S. Minemoto, T. Umegaki, Y. Oguchi, T. Morishita, A. T. Le, S. Watanabe, and H. Sakai, Phys. Rev. A **78**, 061402(R) (2008).

[36] E. J. Takahashi, T. Kanai, Y. Nabekawa, and K. Midorikawa, Appl. Phys. Lett. **93**, 041111 (2008).

[37] P. Colosimo et al., Nat. Phys. **4**, 386 (2008).

[38] J. P. Farrell, L. S. Spector, B. K. McFarland, P. H. Bucksbaum, M. Gühr, M. B. Gaarde, and K. J. Schafer, Phys. Rev. A **83**, 023420 (2011).

[39] J. Higuet et al., Phys. Rev. A **83**, 053401 (2011).

[40] C. Jin, H. J. Wörner, V. Tosa, A. T. Le, J. B. Bertrand, R. R. Lucchese, P. B. Corkum, D. M. Villeneuve, and C. D. Lin, J. Phys. B **44**, 095601 (2011).

[41] J. W. Cooper, Phys. Rev. **128**, 681 (1962).

[42] A. T. Le, R. R. Lucchese, S. Tonzani, T. Morishita, and C. D. Lin, Phys. Rev. A **80**, 013401 (2009).

[43] C. D. Lin, A. T. Le, C. Jin, and H. Wei, J. Phys. B **51**, 104001 (2018).

[44] C. D. Lin, A. T. Le, C. Jin, and H. Wei, *Attosecond and Strong-Field Physics: Principles and Applications* (Cambridge University, Cambridge, England, 2018), pp. 209–213.

[45] A. D. Shiner, B. E. Schmidt, C. Trallero-Herrero, H. J. Wörner, S. Patchkovskii, P. B. Corkum, J.-C. Kieffer, F. Légaré, and D. M. Villeneuve, Nat. Phys. **7**, 464 (2011).

[46] A. D. Shiner, B. E. Schmidt, C. Trallero-Herrero, P. B. Corkum, J.-C. Kieffer, F. Légaré, and D. M. Villeneuve, J. Phys. B **45**, 074010 (2012).

[47] G. Wang, C. Jin, A.-T. Le, and C. D. Lin, Phys. Rev. A **86**, 015401 (2012).

[48] C. Jin and C. D. Lin, Photonics Res. **6**, 434 (2018).

[49] C. Jin, A.-T. Le, and C. D. Lin, Phys. Rev. A **83**, 053409 (2011).

[50] C. Jin, J. B. Bertrand, R. R. Lucchese, H. J. Wörner, P. B. Corkum, D. M. Villeneuve, A.-T. Le, and C. D. Lin, Phys. Rev. A **85**, 013405 (2012).

[51] C. Jin, S.-J. Wang, X. Zhao, S.-F. Zhao, and C. D. Lin, Phys. Rev. A **101**, 013429 (2020).

[52] C. Jin, A. T. Le, and C. D. Lin, Phys. Rev. A **83**, 023411 (2011).

[53] R. R. Lucchese and V. McKoy, Phys. Rev. A **26**, 1406 (1982).

[54] C. Jin, A. T. Le, S. F. Zhao, R. R. Lucchese, and C. D. Lin, Phys. Rev. A **81**, 033421 (2010).

[55] F. A. Gianturco, R. R. Lucchese, and N. Sanna, J. Chem. Phys. **100**, 6464 (1994).

[56] A. P. P. Natalense and R. R. Lucchese, J. Chem. Phys. **111**, 5344 (1999).

[57] C. Jin, A. T. Le, and C. D. Lin, Phys. Rev. A **79**, 053413 (2009).

[58] X. M. Tong, Z. X. Zhao, and C. D. Lin, Phys. Rev. A **66**, 033402 (2002).

[59] S. F. Zhao, C. Jin, A. T. Le, T. F. Jiang, and C. D. Lin, Phys. Rev. A **81**, 033423 (2010).

[60] M. Lein, R. De Nalda, E. Heesel, N. Hay, E. Springate, R. Velotta, M. Castillejo, P. L. Knight, and J. P. Marangos, J. Mod. Opt. **52**, 465 (2005).

[61] H. Stapelfeldt and T. Seideman, Rev. Mod. Phys. **75**, 543 (2003).

[62] J. Ortigoso, M. Rodriguez, M. Gupta, and B. Friedrich, J. Chem. Phys. **110**, 3870 (1999).

[63] J. Levesque, Y. Mairesse, N. Dudovich, H. Pépin, J.-C. Kieffer, P. B. Corkum, and D. M. Villeneuve, Phys. Rev. Lett. **99**, 243001 (2007).

[64] X. Zhou, R. Lock, N. Wagner, W. Li, H. C. Kapteyn, and M. M. Murnane, Phys. Rev. Lett. **102**, 073902 (2009).

[65] A. T. Le, R. R. Lucchese, and C. D. Lin, Phys. Rev. A **82**, 023814 (2010).

[66] A. T. Le and C. D. Lin, J. Mod. Opt. **58**, 1158 (2011).

[67] S. B. Schoun, R. Chirla, J. Wheeler, C. Roedig, P. Agostini, L. F. DiMauro, K. J. Schafer, and M. B. Gaarde, Phys. Rev. Lett. **112**, 153001 (2014).

[68] J. Itatani, D. Zeidler, J. Levesque, M. Spanner, D. M. Villeneuve, and P. B. Corkum, Phys. Rev. Lett. **94**, 123902 (2005).

[69] K.-H. Hong, C.-J. Lai, J. P. Siqueira, P. Krogen, J. Moses, C.-L. Chang, G. J. Stein, L. E. Zapata, and F. X. Kärtner, Opt. Lett. **39**, 3145 (2014).

[70] N. Ishii, K. Kaneshima, K. Kitano, T. Kanai, S. Watanabe, and J. Itatani, Nat. Commun. **5**, 3331 (2014).

[71] S. L. Cousin, F. Silva, S. Teichmann, M. Hemmer, B. Buades, and J. Biegert, Opt. Lett. **39**, 5383 (2014).

[72] S. M. Teichmann, F. Silva, S. L. Cousin, M. Hemmer, and J. Biegert, Nat. Commun. **7**, 11493 (2016).

[73] A. S. Johnson, D. R. Austin, D. A. Wood, C. Brahms, A. Gregory, K. B. Holzner, S. Jarosch, E. W. Larsen, S. Parker, C. S. Strüer, P. Ye, J. W. G. Tisch, and J. P. Marangos, Sci. Adv. **4**, eaar3761 (2018).

[74] C. Jin, M.-C. Chen, H.-W. Sun, and C. D. Lin, Opt. Lett. **43**, 4433 (2018).

[75] J. Li, X. M. Ren, Y. C. Yin, K. Zhao, A. Chew, Y. Cheng, E. Cunningham, Y. Wang, S. Y. Hu, Y. Wu, M. Chini, and Z. Chang, Nat. Commun. **8**, 186 (2017).

[76] T. Gaumnitz, A. Jain, Y. Pertot, M. Huppert, I. Jordan, F. Ardana-Lamas, and H. J. Wöner, Opt. Express **25**, 27506 (2017).

[77] P.-C. Huang, C. Hernández-García, J.-T. Huang, P.-Y. Huang, C.-H. Lu, L. Rego, D. D. Hickstein, J. L. Ellis, A. Jaron-Becker, A. Becker, S.-D. Yang, C. G. Durfee, L. Plaja, H. C. Kapteyn, M. M. Murnane, A. H. Kung, and M.-C. Chen, Nat. Photonics **12**, 349 (2018).